Time evolution of city distributions in Germany

Ikeda, Kiyohiro and Osawa, Minoru and Takayama, Yuki

Tohoku University, Kyoto University, Kanazawa University

1 April 2021

Noname manuscript No.
(will be inserted by the editor)

Time evolution of city distributions in Germany

Group-theoretic spectrum analysis

Kiyohiro Ikeda · Minoru Osawa · Yuki Takayama

Received: date / Accepted: date

Abstract This paper aims to capture characteristic agglomeration patterns in population data in Germany from 1987 to 2011, encompassing pre- and post-unification periods. We utilize a group-theoretic double Fourier spectrum analysis procedure (Ikeda et al., 2018) as a systematic means to capture characteristic agglomeration patterns in population data. Among a plethora of patterns to be self-organized from a uniform state, we focus on a megalopolis pattern, a rhombic pattern, and a core–satellite pattern (a downtown surrounded by hexagonal satellite cities). As the technical contribution of this paper, we newly introduce a *principal vector* as a superposition of these patterns in order to grasp the multi-scale nature of agglomerations. Benchmark spectra for these patterns are advanced and are found in the population data of Germany in 2011. An incremental population is investigated using this principal vector to successfully detect a shift of predominant population increase/decrease patterns in the pre- and post-unification periods.

Keywords Central place theory · City distribution · Core–satellite pattern · German reunification · Hexagons · Megalopolis · Spectrum analysis

Grant-in-Aid for JSPS 18K04380/18K18874/19K15108 is greatly appreciated.

K. Ikeda (Corresponding Author)
Department of Civil and Environmental Engineering, Tohoku University, Aoba, Sendai 980-8579, Japan
Tel.: +81-22-795-7416
Fax: +81-22-795-7418
E-mail: kiyohiro.ikeda.b4@tohoku.ac.jp
ORCID 0000-0002-0291-4346

M. Osawa
Department of Civil and Environmental Engineering, Tohoku University, Aoba, Sendai 980-8579, Japan

Y. Takayama
Institute of Science and Engineering, Kanazawa University, Kakuma, Kanazawa 920-1192, Japan

1 Introduction

In this paper, a systematic methodology to capture characteristic agglomeration pattens in population data is proposed using and extending a group-theoretic double Fourier spectrum analysis procedure (Ikeda et al., 2018). This methodology is put to use in the population data in Germany during the pre- and post-reunification periods (from 1987 to 2010) to demonstrate the occurrence of a phase shift in the predominant agglomeration pattern.

Christaller (1933) envisaged the existence of hexagonal distributions of cities and towns in Southern Germany. Thereafter, several attempts to simulate the self-organization of central place systems have been conducted through modeling of economic mechanisms of agglomerations (e.g., Eaton and Lipsey, 1975; Clarke and Wilson, 1983; Sanglier and Allen, 1989; Munz and Weidlich, 1990; Fujita et al., 1999; Tabuchi and Thisse, 2011; Banaszak et al., 2015). Hexagonal patterns on a hexagonal lattice were shown to exist theoretically and were numerically simulated (Ikeda and Murota, 2014; Ikeda et al., 2014, 2017). The reemergence of central place theory with its complements, such as NEG models, has come to be acknowledged (Mulligan et al., 2012). Bridging empirics and theory is regarded as an important topic (e.g., Stelder, 2005; Bosker et al., 2010). The evolution of network analysis in geography was reviewed by Ducruet and Beauguitte (2014). The role of spatial topology in the core-periphery model was studied by Barbero and Zofío (2016). There are studies related to Germany, which is the target of this paper: German division and reunification by Redding and Sturm (2008) and the city size distribution of West Germany by Bosker et al. (2008) and Findeisena and Südekum (2008).

Despite these studies, the measuring of spatial agglomeration patterns in actual population data remains a difficult problem. As described in central place theory (Christaller, 1933; Lösch, 1940), the real-world spatial agglomeration patterns form the hierarchical structure of centers and subcenters. As a result, measurement becomes scale-dependent; in data at a given scale, some centers can be easily identified while some lower-level subcenters are not.

As an attempt to handle such a multi-scale nature of spatial agglomeration patterns and to capture characteristic agglomeration patterns in population data with a lot of noise, Ikeda et al. (2018) introduced the group-theoretic Fourier analysis and found hexagonal patterns in population data in Southern Germany and Eastern USA. In this work, a hexagonal lattice was employed in line with the seminal works of Christaller (1933) and Lösch (1940). Moreover, they elaborately assembled the Fourier basis into several groups to express hexagonal modes to be self-organized from the uniform state, as envisaged in central place theory. The difference in the spatial frequency of the Fourier modes is used to express different levels of city hierarchy in the underlying central place system. This contrasts with a customary double Fourier series in a square lattice that cannot express such self-organizing hexagons. The basis vectors of the group-theoretic Fourier series were found to coincide with the eigenvectors of an adjacency matrix in spatial statistics, which are known to capture distinctive spatial patterns with associated spatial autocorrelation distances (Tiefelsdorf and Griffith, 2007). Then the Fourier terms associated with negative eigenvalues of the adjacency matrix were cut to filter noise in the population data.

This paper aims to capture characteristic agglomeration patterns in population data in Germany from 1987 to 2011, using and extending the spectrum analysis procedure by Ikeda et al. (2018). First, as the technical contribution of this paper, we newly introduce a *principal vector* as a superposition of a few Fourier modes in order to grasp the multi-scale nature of agglomerations. Modes with the first few largest eigenvalues of the adjacency matrix are used in the principal vector not only to filter noise but to capture important agglomeration patterns. Next, we set forth a megalopolis pattern, a rhombic pattern, and a core–satellite pattern (a downtown surrounded by hexagonal satellite cities) as the target of the spectrum analysis and observe benchmark spectra for these patterns. We found that only four spectra are predominant for these three prototype patterns. Such predominant spectra are actually found in the population data in Germany in 2011 and agglomeration patterns are successfully grasped by the principal vector with only these four terms, while Ikeda et al. (2018) employed as many as 15 modes as candidates. Last, an incremental population during the pre- and post-reunification periods (from 1987 to 2011) is investigated to detect a shift of the predominance of a megalopolis pattern around Frankfurt to that of a core-satellite pattern for several large cities.

This paper is organized as follows. Group-theoretic spectrum analysis procedure is presented in Section 2. Hexagonal distributions of cities are detected in the population data of Germany in Section 3.

2 Group-theoretic Fourier spectrum analysis

We introduce the bifurcation mechanism of the self-organizing hexagons on an $n \times n$ hexagonal lattice with periodic boundary conditions and an oblique discrete Fourier series on this lattice, as a summary of Ikeda and Murota (2014) and Ikeda et al. (2018). It is to be emphasized that this Fourier series was elaborately constructed so as to be compatible with the bifurcation mechanism to engender hexagonal patterns, whereas a more customary double Fourier series in a square lattice lacks in such compatibility.

2.1 Group-theoretic Fourier series and self-organizing patterns

An $n \times n$ finite hexagonal lattice with periodic boundary conditions represents uniformly distributed $n \times n$ discrete places (see Fig. 1 for an example of $n = 3$). The places are indexed by (n_1, n_2) and the population distribution vector is indexed as

$$\boldsymbol{\lambda} = (\lambda_{n_1 n_2} \mid n_1, n_2 = 0, \ldots, n-1).$$

The population distribution vector $\boldsymbol{\lambda}$ on the $n \times n$ hexagonal lattice (n is a multiple of 6) can be expanded to a group-theoretic oblique discrete Fourier series as (Ikeda and Murota, 2014)

$$\begin{aligned}\boldsymbol{\lambda} = &\sum_{m=1}^{3}\sum_{i=1}^{m} c_i^{(m)} \boldsymbol{q}_i^{(m)} + \sum_{k=1}^{n/2-1}\sum_{i=1}^{6} c_i^{(k,0)} \boldsymbol{q}_i^{(k,0)} + \sum_{k=1}^{n/2-1,\ k\neq n/3}\sum_{i=1}^{6} c_i^{(k,k)} \boldsymbol{q}_i^{(k,k)} \\ &+ \sum_{1\le \ell \le k-1,\ 2k+\ell \le n-1}\ \sum_{i=1}^{12} c_i^{(k,\ell)} \boldsymbol{q}_i^{(k,\ell)} \end{aligned} \tag{1}$$

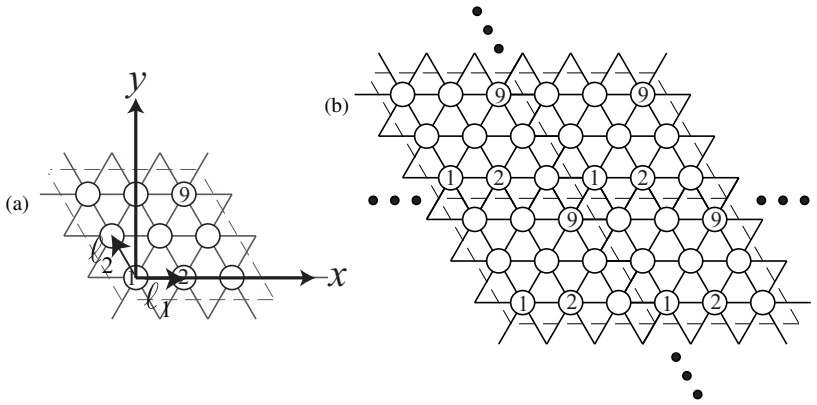

Fig. 1: (a) 3×3 hexagonal lattice. (b) Spatially repeated 3×3 hexagonal lattices using periodic boundary conditions.

with Fourier coefficients $c_i^{(m)}$ and $c_i^{(k,\ell)}$. This is not a naïve Fourier series but is elaborately rearranged and regrouped associated with the bifurcation mechanism. In (1), k and ℓ denote wave numbers of the Fourier basis vectors, which are given by

$$
\begin{aligned}
&\boldsymbol{q}_1^{(1)} = \frac{1}{n}(1,\dots,1)^\top = \langle 1\rangle,\\
&[\boldsymbol{q}_1^{(2)}, \boldsymbol{q}_2^{(2)}] = [\ \langle\cos(2\pi(n_1-2n_2)/3)\rangle,\ \langle\sin(2\pi(n_1-2n_2)/3)\rangle\ ],\\
&[\boldsymbol{q}_1^{(3)}, \boldsymbol{q}_2^{(3)}, \boldsymbol{q}_3^{(3)}] = [\ \langle\cos(\pi n_1)\rangle,\ \langle\cos(\pi n_2)\rangle,\ \langle\cos(\pi(n_1-n_2))\rangle\ ],\\
&[\boldsymbol{q}_1^{(k,0)},\dots,\boldsymbol{q}_6^{(k,0)}]\\
&\quad = [\ \langle\cos(2\pi k\, n_1/n)\rangle,\ \langle\sin(2\pi k\, n_1/n)\rangle,\ \langle\cos(2\pi k(-n_2)/n)\rangle,\\
&\qquad \langle\sin(2\pi k(-n_2)/n)\rangle,\ \langle\cos(2\pi k(-n_1+n_2)/n)\rangle,\ \langle\sin(2\pi k(-n_1+n_2)/n)\rangle\ ]\\
&\qquad\qquad\qquad\qquad \text{for } 1 \le k \le \frac{n}{2}-1,\\
&[\boldsymbol{q}_1^{(k,k)},\dots,\boldsymbol{q}_6^{(k,k)}]\\
&\quad = [\ \langle\cos(2\pi k(n_1+n_2)/n)\rangle,\ \langle\sin(2\pi k(n_1+n_2)/n)\rangle,\ \langle\cos(2\pi k(n_1-2n_2)/n)\rangle,\\
&\qquad \langle\sin(2\pi k(n_1-2n_2)/n)\rangle,\ \langle\cos(2\pi k(-2n_1+n_2)/n)\rangle,\ \langle\sin(2\pi k(-2n_1+n_2)/n)\rangle\ ]\\
&\qquad\qquad\qquad\qquad \text{for } 1 \le k \le \frac{n}{2}-1,\ k \ne \frac{n}{3},\\
&[\boldsymbol{q}_1^{(k,\ell)},\dots,\boldsymbol{q}_{12}^{(k,\ell)}]\\
&\quad = [\ \langle\cos(2\pi(kn_1+\ell n_2)/n)\rangle,\ \langle\sin(2\pi(kn_1+\ell n_2)/n)\rangle,\ \dots\\
&\qquad \langle\cos(2\pi(-(k+\ell)n_1+\ell n_2)/n)\rangle,\ \langle\sin(2\pi(-(k+\ell)n_1+\ell n_2)/n)\rangle\ ]\\
&\qquad\qquad\qquad\qquad \text{for } 1 \le \ell \le k-1,\ 2k+\ell \le n-1.
\end{aligned}
$$

Here, for a vector $(g(n_1,n_2) \mid n_1,n_2 = 0,1,\dots,n-1)$, we use the notation $\langle g(n_1,n_2)\rangle$ for its normalization ($\|\langle g(n_1,n_2)\rangle\| = 1$).

Self-organizing bifurcating patterns from a uniform state ($\boldsymbol{q}_1^{(1)} \equiv \langle 1,\dots,1\rangle^\top$) were presented (Ikeda and Murota, 2014). We are particularly interested in a core–satellite pattern and a series of hexagons in central place theory. These patterns are given by special combinations of the basis vectors as

$$
\boldsymbol{q}^{\mu}_{\text{hexa}} = \begin{cases} \boldsymbol{q}^{(2)}, \\ \boldsymbol{q}_1^{(3)} + \boldsymbol{q}_2^{(3)} + \boldsymbol{q}_3^{(3)}, \\ \boldsymbol{q}_1^{(k,\ell)} + \boldsymbol{q}_3^{(k,\ell)} + \boldsymbol{q}_5^{(k,\ell)} \quad (\ell = 0 \text{ or } k), \\ \displaystyle\sum_{i=1}^{6} \boldsymbol{q}_{2i-1}^{(k,\ell)}. \end{cases} \tag{2}
$$

Here μ is either (1), (2), (3), or (k,ℓ). Some of these hexagons are shown in Fig. 2.

In addition to these hexagons, a "core–satellite pattern" (Fig. 2(d)) for $\boldsymbol{q}^{(2,1)}_{\text{hexa}}$ plays a vital role in the search for distributions of cities. This pattern represents a circle (core place) surrounded by six smaller ellipses (periphery places).

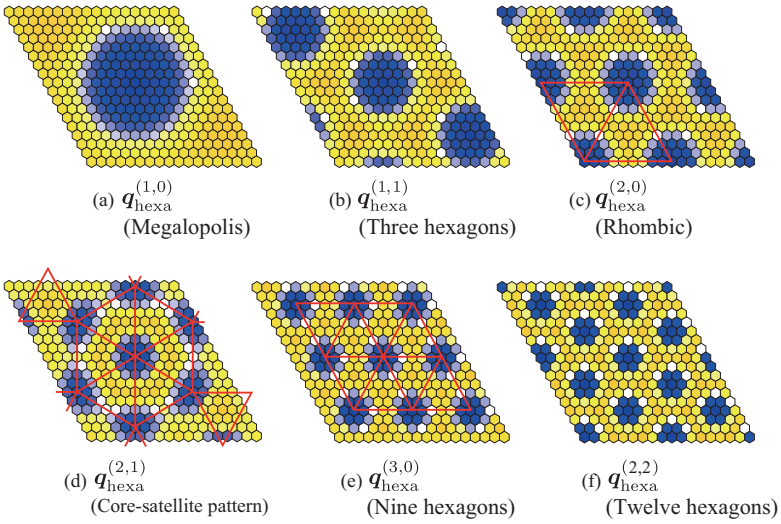

Fig. 2: Hexagonal and core–satellite patterns (shifted to the center of the domain) on an 18×18 hexagonal lattice. A blue hexagonal area denotes a positive component, a yellow one indicates a negative one, the magnitude of the component increases as the color becomes darker, and a red line is used to clarify spatial patterns.

2.2 Group-theoretic spectrum analysis procedure

A group-theoretic spectrum analysis procedure is introduced in this section as a systematic tool to capture characteristic agglomeration patterns in the statistical data of population (Section 3).

We reassemble the double Fourier components[1] in (1) as

$$\boldsymbol{q}^{\mu} = \sum_{i=1}^{M(\mu)} c_i^{\mu} \boldsymbol{q}_i^{\mu}, \quad \mu \in R, \tag{3}$$

in which μ is either (1), (2), (3), or (k, ℓ), R is the whole set of μ, and $M(\mu)$ (= 1, 2, 3, 6, or 12) is the number of basis vectors $\boldsymbol{q}_i^{\mu}$ for μ. This assemblage is compatible with the bifurcation mechanism (Section 2.1), and the vector $\boldsymbol{q}^{\mu}$ for appropriately chosen c_i^{μ} can represent hexagonal patterns $\boldsymbol{q}^{\mu}_{\mathrm{hexa}}$ in (2). Then the double Fourier series in (1) is rewritten as

$$\boldsymbol{\lambda} = \sum_{\mu \in R} \boldsymbol{q}^{\mu}. \tag{4}$$

This is employed in the spectrum analysis (Section 3).

The component vectors $\boldsymbol{q}^{\mu}$ of (4) depicted in Fig. 2 do indeed look like agglomeration patterns. Yet some component vectors with high spatial frequencies (e.g, Fig 3)

[1] These are so-called *isotypic components* in group-theoretic bifurcation theory (Golubitsky et al., 1988).

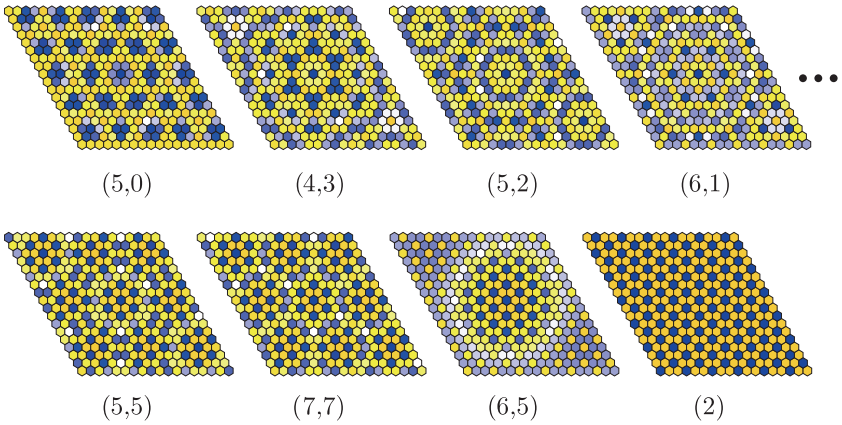

Fig. 3: Hexagonal patterns with higher frequencies associated with the eigenvectors on an 18×18 hexagonal lattice. A blue hexagonal area denotes a positive component, a yellow one indicates a negative one, and the magnitude of the component increases as the color becomes darker.

are not realistic as spatial agglomeration patterns. To filter such vectors, we resort to an adjacency matrix that has come to be used in spatial statistical studies (Dray et al., 2006; Murakami and Griffith, 2015). Eigenvectors of this matrix corresponding to large eigenvalues are known to capture cluster or agglomeration effects (Tiefelsdorf and Griffith, 2007), which the central place theory describes. In our analysis, these eigenvectors, which are often called spatial eigenvectors, are put to use in the selection of the principal components that can express agglomeration effects.

An adjacency matrix $A = \{a_{ij} \mid i, j = 1, \ldots, N\}$ of the $n \times n$ hexagonal lattice network, which is defined as $a_{ij} = 1$ if i and j are connected and $a_{ij} = 0$ otherwise, takes the form:

$$A = \begin{pmatrix} B & C & & C^\top \\ C^\top & B & \ddots & \\ & \ddots & \ddots & C \\ C & & C^\top & B \end{pmatrix} \tag{5}$$

with

$$B = \begin{pmatrix} 1 & & 1 \\ 1 & \ddots & \\ & \ddots & 1 \\ 1 & & 1 \end{pmatrix}, \quad C = \begin{pmatrix} 1 & 1 & & \\ & \ddots & \ddots & \\ & & 1 & 1 \\ 1 & & & 1 \end{pmatrix}. \tag{6}$$

It is noteworthy that the eigenvectors $\boldsymbol{q}_i^\mu$ of A are also the eigenvectors of the Jacobian matrix J of the governing equation, thereby related to self-organizing patterns (Ikeda et al., 2018).

With resort to the eigenvalues $\xi^\mu = (\boldsymbol{q}_i^\mu)^\top A \boldsymbol{q}_i^\mu$ of the adjacent matrix A, we would like to depict a subset for large eigenvalues, that is,

$$R^* = \{\mu \mid \xi^\mu \geq \xi^* \text{ and } \mu \neq (1)\} \tag{7}$$

as principal components for some threshold value ξ^*; $\mu = (1)$ associated with the uniform distribution is excluded here and in the remainder of this paper since we target not uniformity but heterogeneity due to spatial agglomerations. Then we define the *principal vector* for these components as

$$\boldsymbol{q}_m^* = \sum_{\mu \in R^*} \boldsymbol{q}^\mu, \tag{8}$$

where m denotes the number of terms involved in the summation on the right hand side. In application, it is vital to choose the number m of the terms appropriately as $\boldsymbol{q}_m^*$ with too small m may fail to capture spatial distribution property and $\boldsymbol{q}_m^*$ with too large m is subject to noise.

The eigenvalues ξ^μ of the adjacent matrix A for an 18×18 lattice ($n = 18$) are listed in Table 1 in a decreasing order. The eigenvectors with larger wave numbers k and ℓ, which have higher spatial frequencies with a larger number of agglomerated zones, tend to have smaller eigenvalues. These eigenvectors with noise-like patterns (Fig. 3) are systematically excluded by focusing on the principal components in (7). The hexagonal and core–satellite patterns in Figs. 2(a)–(d) are associated with the first to the fourth largest positive eigenvalues and play an important role in the description of the real population data (Section 3), whereas those in Figs. 2(e)–(f) associated with the fifth to the sixth largest positive eigenvalues are presented here for reference.

Table 1: Order of the eigenvalues ξ^{μ} of the 18×18 adjacency matrix A (Ikeda et al., 2018)

Order	μ	Eigenvalue	Name	Corresponding figure
1	(1,0)	5.76	Megalopolis	Fig. 2(a)
2	(1,1)	5.29	Three hexagons	Fig. 2(b)
3	(2,0)	5.06	Rhombic	Fig. 2(c)
4	(2,1)	4.41	Core satellite	Fig. 2(d)
5	(3,0)	4.00	Nine hexagons	Fig. 2(e)
6	(2,2)	3.41	Twelve hexagons	Fig. 2(f)
7	(3,1)	3.23		
8	(4,0)	2.69		
9	(3,2)	2.18		
10	(4,1)	1.88		
11	(5,0)	1.31		
12	(3,3)	1.00		
13	(4,2)	0.88		
14	(5,1)	0.53		
15	(6,0)	0.00		
16	(4,3)	−0.18		
17	(5,2)	−0.35		
18	(6,1)	−0.65		
19	(7,0)	−1.06		
20	(4,4)	−1.18		
21	(5,3)	−1.23		
22	(6,2)	−1.35		
23	(7,1)	−1.53		
24	(8,0)	−1.76		
25–29	(5,4), (7,2), (6,3), (8,1)	−2.00		
	(3)	−2.00	$k = 4$ system	
30	(8,8)	−2.23		
31	(7,3)	−2.41		
32	(6,4)	−2.53		
33	(5,5)	−2.57		
34	(7,7)	−2.72		
35	(6,5)	−2.88		
36	(2)	−3.00	$k = 3$ system	

2.3 Benchmark spectra for important spatial patterns

In preparation for the application of the spectrum analysis to real data, we set forth a megalopolis pattern, a rhombic pattern, and a core–satellite pattern (a downtown surrounded by hexagonal satellite cities) in Fig. 2 as the target of the spectrum analysis and observe benchmark spectra for these three patterns. In particular, we would like to determine a sufficient number m of terms to be included in the principal vector $\boldsymbol{q}^*_m = \sum_{\mu\in R^*} \boldsymbol{q}^\mu$ in (8) to express these patterns unambiguously.

Megalopolis patterns are shown at the left of Fig. 4, whereas the associated group-theoretic Fourier spectra are shown at the right. The full agglomeration in Fig. 4(a) displays an almost flat spectrum distribution without a predominant spectrum. When the patterns become more diffused from (b) to (c), we can see the predominance of the spectrum for $(k,\ell) = (1,0)$ accompanied by that for $(1,1)$ as the second largest one. We can thus regard the predominance of the spectrum of $(1,0)$ to signify the presence of a megalopolis pattern, whereas the emergence of the spectrum of $(1,1)$ as its byproduct.

A core–satellite pattern and its spectrum are shown in Fig. 5(a). We can see the emergence of the predominant spectrum $(k,\ell) = (2,1)$, whereas even the second and the third predominant ones for $(1,1)$ and $(4,0)$ are quite small in magnitudes. This is an idealistic benchmark for a core–satellite pattern. By contrast, real data often features two predominant spectra for $(k,\ell) = (2,1)$ and $(1,0)$ (cf., Fig. 9(c) and also Ikeda et al., 2018). As a possible scenario of this, we consider the development of an industrial belt between the core place and a satellite place in the core–satellite pattern shown in Figs. 5(b) and (c). In association with the formation of an industrial belt from (a), via (b), to (c), we can see the predominance of the spectrum for $(2,1)$ with byproducts of the spectra for $(1,0)$ and $(1,1)$.

For the rhombic pattern (four hexagons) shown in Fig. 6(a), $(2,0)$ has the largest spectrum. In the patterns in Figs. 6(b) and (c), for which one city has larger population in comparison with the other three cities, the spectra for $(1,0)$ and $(2,0)$ are predominant and the spectrum for $(1,1)$ appears as a byproduct.

Thus the spectra for $(k,\ell) = (1,0)$, $(1,1)$, $(2,0)$, and $(2,1)$ can characterize the existence of spatial patterns of megalopolis, core–satellite, rhombic, and so on. Moreover, these four spectra correspond to the first to the fourth largest eigenvalues of the adjacency matrix A (Table 1). Accordingly, we choose the principal vector in (8) as

$$\boldsymbol{q}^*_4 = \sum_{\mu\in R^*} \boldsymbol{q}^\mu, \qquad R^* = \{(1,0),(1,1),(2,0),(2,1)\}. \tag{9}$$

The spatial patterns expressed by the principal vectors $\boldsymbol{q}^*_4$ for the megalopolis, core–satellite, and rhombic patterns are depicted in Fig. 7(a)–(c) and are capable of capturing their agglomeration properties. We employ the principal vector $\boldsymbol{q}^*_4$ determined in this manner to the spectrum analysis of Germany in Section 3, for which $\boldsymbol{q}^*_4$ is ensured to contain sufficient number of terms in comparison with $\boldsymbol{q}^*_m$ ($m \geq 5$).

In particular, the principal vector $\boldsymbol{q}^*_4$ is suitable for the description of the industrial belt pattern in Fig. 7(d), which is a superposition of the megalopolis pattern $\boldsymbol{q}^{(1,0)}$ and the core–satellite pattern $\boldsymbol{q}^{(2,1)}$, and cannot be expressed only by an individual pattern. In this regard, the principal vector $\boldsymbol{q}^*_m$ is suitable for the description of real data, in which mixed patterns with different sizes are often observed (Section 3).

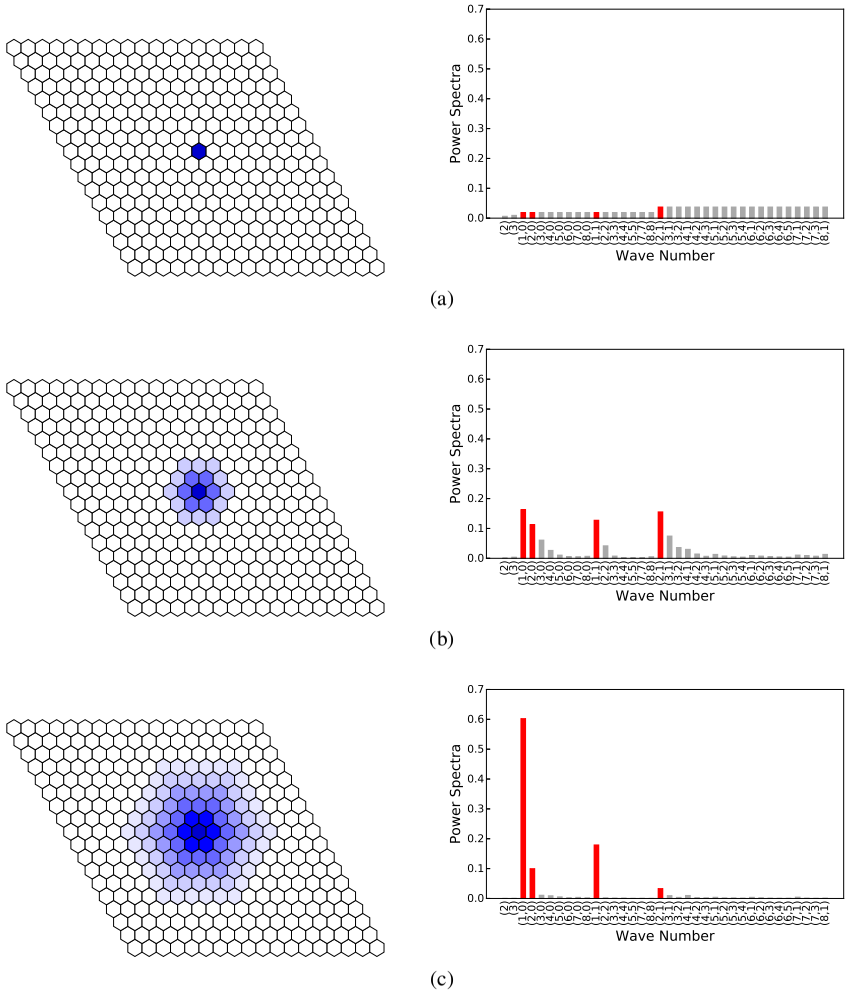

Fig. 4: Megalopolis patterns and their spectra. At the left, the magnitude of the component increases as the blue color becomes darker. At the right, the red bars correspond to the spectra with the first to the fourth largest eigenvalues ξ^{μ} and the brown bars to others.

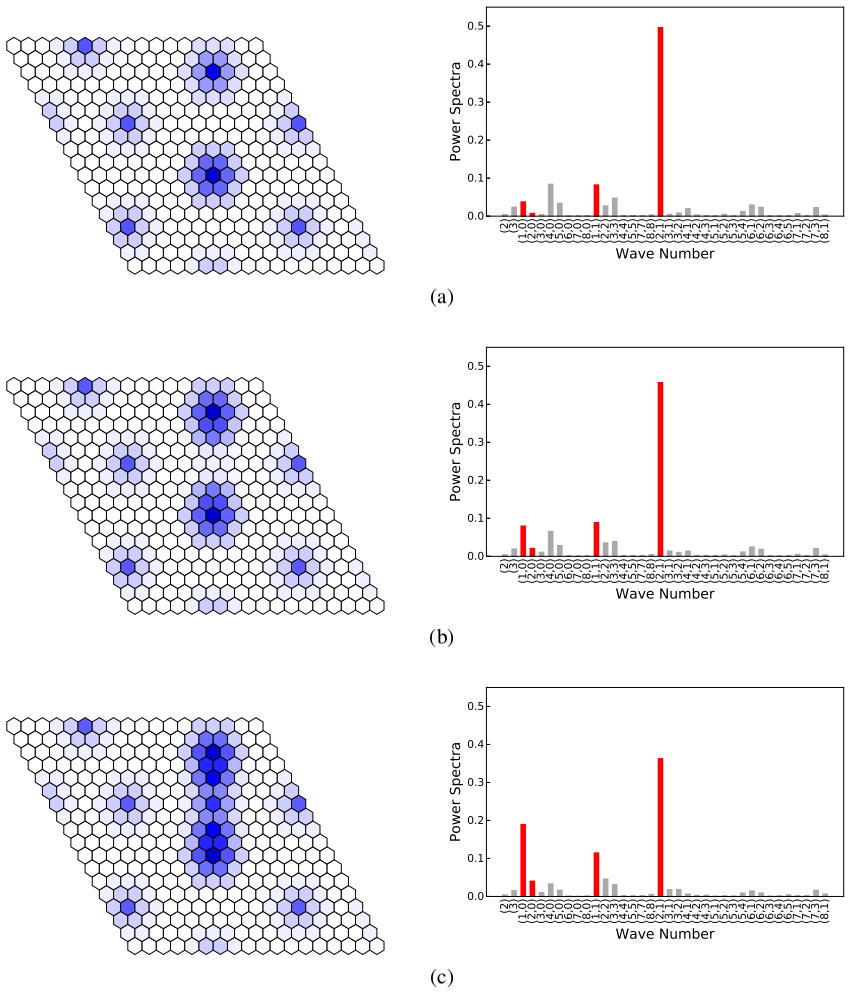

Fig. 5: Emergence of an industrial belt for a core–satellite pattern and evolution of spectra. At the left, the magnitude of the component increases as the blue color becomes darker. At the right, the red bars correspond to the spectra with the first to the fourth largest eigenvalues ξ^{μ} and the brown bars to others.

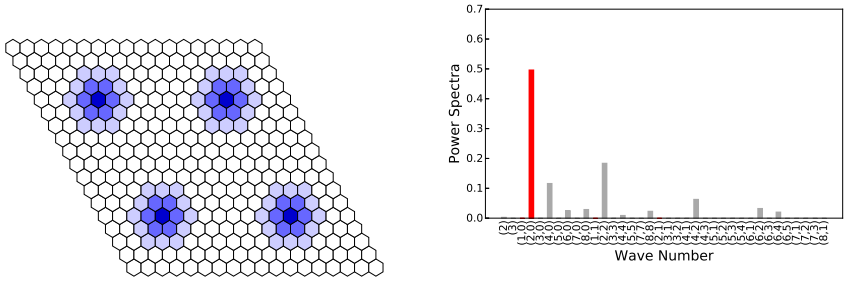

(a) Four identical cities

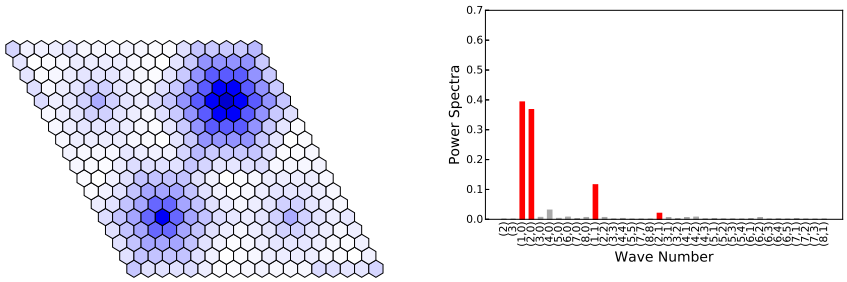

(b) One large, one middle-size, and two small cities

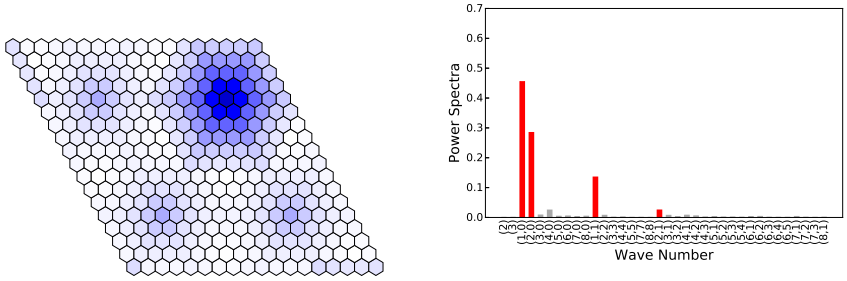

(c) One large and three small cities

Fig. 6: Rhombic patterns and evolution of spectra. At the left, the magnitude of the component increases as the blue color becomes darker. At the right, the red bars correspond to the spectra with the first to the fourth largest eigenvalues ξ^{μ} and the brown bars to others.

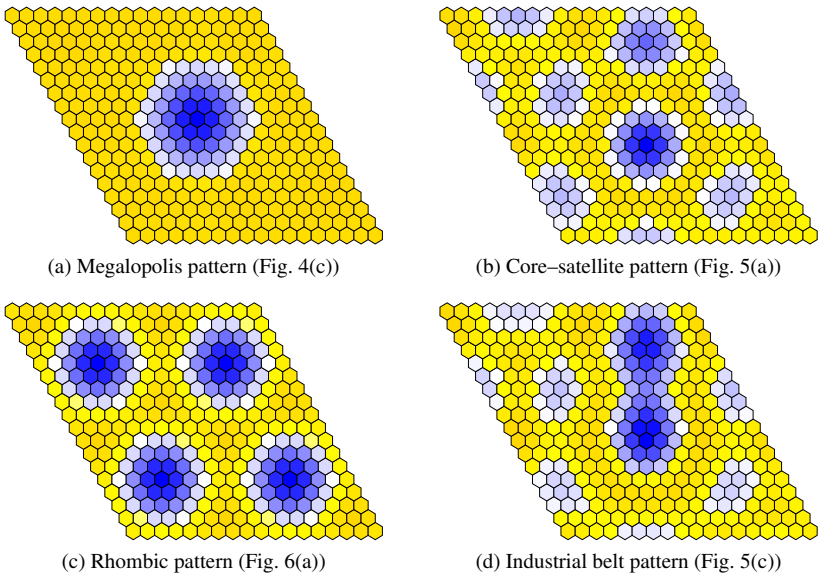

(a) Megalopolis pattern (Fig. 4(c))

(b) Core–satellite pattern (Fig. 5(a))

(c) Rhombic pattern (Fig. 6(a))

(d) Industrial belt pattern (Fig. 5(c))

Fig. 7: The principal vector $\boldsymbol{q}_4^*$ for spatial patterns. A blue hexagonal area denotes a positive component, a yellow one indicates a negative one, and the magnitude of the component increases as the color becomes darker.

3 Group-theoretic spectra for hexagonal distributions of cities in Germany

Although hexagonal distributions of cities and towns in Southern Germany were envisaged by Christaller (1933), the existence of such distributions in the real world remains to be verified in a more systematic manner. As a step towards this verification, a core–satellite pattern in Southern Germany in the population data in 2011 was sought for in Ikeda et al. (2018). In this paper, this search is extended twofold: (1) the area for search is extended northwards and (2) the time evolution of the spectra between 1987–2011, which comprises an era of post-reunification, is investigated.

As a methodological contribution of this paper, the principal vector $\boldsymbol{q}^*_m$ in (8), which is a sum of several vectors $\boldsymbol{q}^\mu$ in (3), is introduced to capture spatial patterns, whereas Ikeda et al. (2018) relied solely on an individual $\boldsymbol{q}^\mu$, which is an authentic self-organizing pattern bifurcating from the uniform state. The usefulness and superiority of $\boldsymbol{q}^*_m$ is to be demonstrated in the remainder of this section. Based on the benchmark spectrum analysis in Section 2.3, we employ $\boldsymbol{q}^*_4$ ($m = 4$) in (9) as the principal vector to capture characteristic agglomerations.

3.1 Setting of the group-theoretic spectrum analysis

We employ the population data map shown in Fig. 8 obtained using the Mercator projection. This map contains Germany and neighboring countries. Fig. 8 (a) denotes the population in 2011, (b) the increment of population during 1987 to 2000,[2] and (c) that during 2000 to 2011. During this period, Germany underwent an up and down of

[2] Although the population map in Eastern Germany is not fully covered due to the lack of data in 1987, it does not affect the results of this section.

Table 2: Original sources of population data.

Country	Data bank (Date, Type) and Internet address
Germany	Statistisches Bundesamt Deutschland (1987/5/25, Census; 2001/12/31, Estimate; 2011/05/09, Census) https://www.destatis.de/EN/Homepage.html
Austria	Statistik Austria (1991/5/15, 2001/5/15, 2011/10/31, Census) http://www.statistik.at/web_de/statistiken/index.html
Belgium	Statistics Belgium (2010/01/01,Estimate) http://statbel.fgov.be/en/statistics/figures/
France	Institut National de la Statistique et des Études Économiques (1990/3/5, 1999/3/8, Census; 2012/01/01, Estimate) http://www.insee.fr/fr/
Netherlands	Centraal Bureau voor de Statistiek (2011/01/01,Estimate) http://statline.cbs.nl/StatWeb/publication/?VW=T&DM=SLNL&PA=70233ned&LA=NL
Switzerland	Swiss Statistics (1990/12/4, 2000/12/5, 2010/12/31, Census) http://www.bfs.admin.ch/bfs/portal/en/index.html
Luxembourg	Le Portail des Statistiques du Luxembourg (1991/3/1, 2001/2/15, 2011/02/01, Census) http://www.statistiques.public.lu/en/index.html

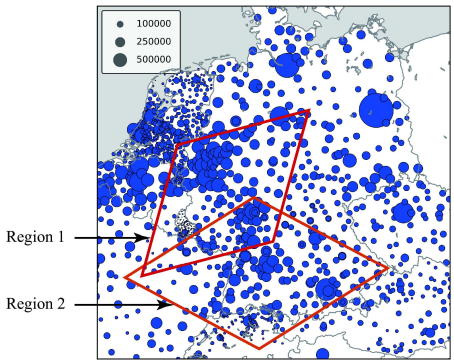

(a) Population in 2011

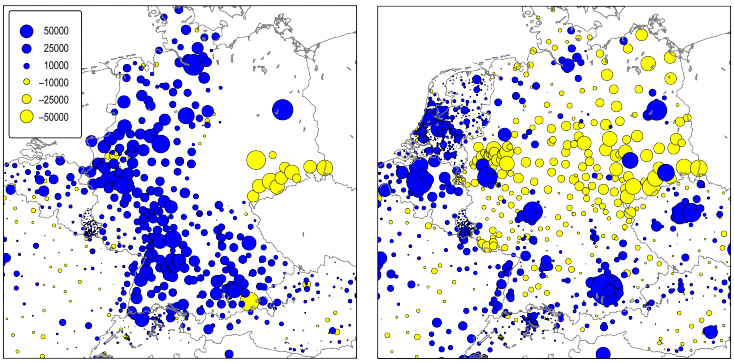

(b) Increment between 1987 to 2000 (c) Increment between 2000 to 2011

Fig. 8: The population data map for Germany and neighboring countries. In (a), a blue circle denotes the size of population. In (b) and (c), a blue circle denotes a positive component, a yellow circle indicates a negative one, and the area of a circle expresses the magnitude of the incremental population.

population from 77.7 million, via 82.1 million, to 80.2 million. We can see an overall increase of population shown by blue circles in Western Germany during 1987 to 2000; however, there is a mixture of increase and decrease (shown by yellow circles) there during 2000 to 2011.

The population data were taken from the City Population website (http://www.citypopulation.de/), which is based on the original sources listed in Table 2. The latitude and longitude of a location were acquired by GoogleMap and Nominatim of OpenStreetMap (https://nominatim.openstreetmap.org/).

On the map in Fig. 8(a), two rhombic regions, which cover most of Germany, were chosen based on a series of preliminary analyses: Region 1 encompassing Southern Germany and Region 2 encompassing Middle Germany. These regions were overlaid by an 18×18 regular-triangular mesh and the population was allocated to the nearest node to arrive at the discretized population distribution (e.g., Fig. 9(b) for Region 1).

3.2 Southern Germany (Region 1) in 2011

Group-theoretic Fourier spectrum analysis of the discretized population data in Fig. 9(b) of Southern germany (Region 1) in 2011 was conducted to obtain the spectrum in Fig. 9(c),[3] which plots the squared magnitudes $\|\boldsymbol{q}^{\mu}\|^2$ ($\mu \in R$) of the assembled Fourier terms in (4); the red bars correspond to the spectra for ξ^{μ} with the first to the fourth largest eigenvalues.

There are two distinct peaks of the spectrum for the megalopolis pattern $\boldsymbol{q}^{(1,0)}$ and for the core–satellite pattern $\boldsymbol{q}^{(2,1)}$, similarly to the benchmark spectrum for the industrial belt for a core–satellite pattern (Fig. 5(c)). The megalopolis pattern in Fig. 9(d) expresses a large agglomeration along an industrial belt between Frankfurt and Stuttgart. The core–satellite pattern in Fig. 9(e) with seven blue circular or elliptic zones captures agglomeration at the four larger cities, München, Frankfurt, Stuttgart, and Nürnberg, which form a clear rhombic shape. Saarbrücken is another place of agglomeration in this pattern. Yet we encounter a problem in that Zürich is located at the middle of two elliptic zones of agglomeration, which express a chain of cities: Konstanz, Zürich, and Mulhouse. Thus the core–periphery pattern is deviated from the real population distribution in the south, although it is an authentic self-organizing pattern bifurcating from the uniform state.

In a further search of agglomeration patterns, we resort to the principal vector $\boldsymbol{q}^*_m$ in (8). Recall that

$$\boldsymbol{q}^*_4 = \sum_{\mu \in R^*} \boldsymbol{q}^{\mu}, \qquad R^* = \{(1,0),(1,1),(2,0),(2,1)\}$$

in (9) with $m = 4$ terms is set forth to characterize agglomeration patterns based on the analysis of the benchmark spectra (Section 2.3). The spatial patterns $\boldsymbol{q}^{\mu}$ for $\mu = (1,0),(1,1),(2,0)$, and $(2,1)$ are presented in Figs. 9(d)–(g) and those for $\mu = (3,0)$ and $(2,2)$ in (h) for reference.

In order to testify the sufficiency the use of $m = 4$ terms, the vector $\boldsymbol{q}^*_m$ for the present case is observed for various values of m, as depicted in Fig. 10; the pattern for $\boldsymbol{q}^*_4$ looks quite close to that for $\boldsymbol{q}^*_5$, thereby ensuring that $m = 4$ is already large enough to grasp agglomeration characteristics. Note that the number $m = 4$ is very small in comparison with the total number of 18×18 ($= 324$) terms of the Fourier analysis. The distribution becomes more scattered for larger m ($= 15, 35$).

The principal vector $\boldsymbol{q}^*_4$ (Fig. 11(a)), which is the superposition of these four components, displays several blue circular or elliptic zones of agglomeration. This expresses a spatial pattern for which Stuttgart is surrounded by several agglomerated places: Frankfurt, Nürnberg, München, Zürich, an so on. This pattern is close to the pattern envisaged by Christaller (Fig. 11(b)), in which Stuttgart is surrounded by five places. Thus the principal vector proposed in this paper is capable of capturing spatial agglomeration patterns, and is more flexible than the use of a single term $\boldsymbol{q}^*_1$ in Ikeda et al. (2018), in which $\boldsymbol{q}^{(2,1)}$ for the core–periphery pattern was chosen as the predominant pattern and the number of satellite places were fixed to be six.

[3] In this figure and in the remainder of this paper, the squared magnitude $\|\boldsymbol{q}^{(1)}\|^2$ for the uniform distribution is suppressed since such a distribution is not of interest in the present study.

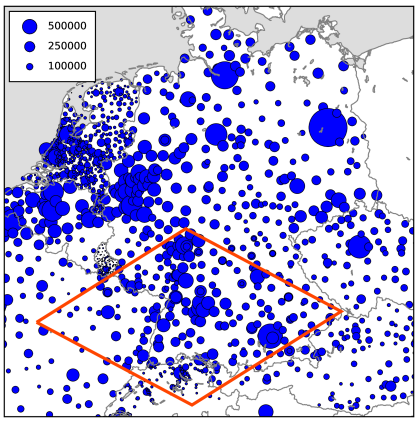

(a) Population map and Region 1 (red rhombus)

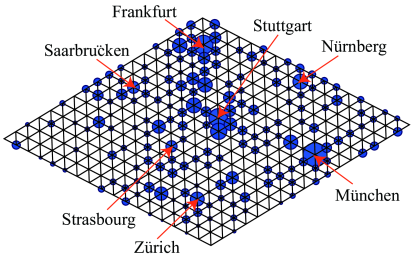

(b) Discretized population

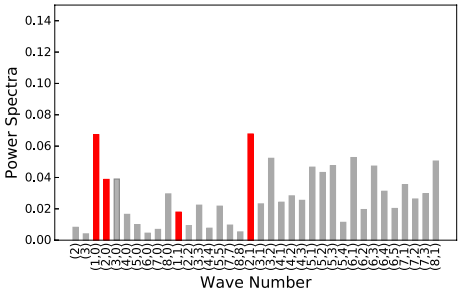

(c) Spectrum

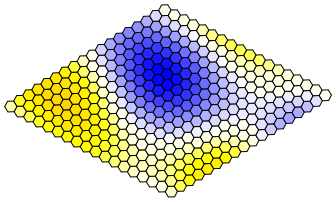

(d) $\boldsymbol{q}^{(1,0)}$ (Megalopolis, 1st largest ξ^{μ})

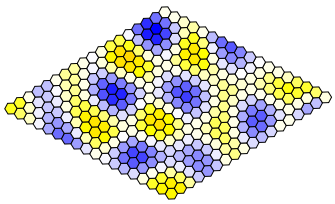

(e) $\boldsymbol{q}^{(2,1)}$ (Core–satellite, 4th largest ξ^{μ})

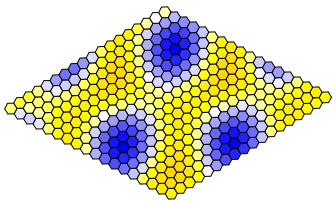

(f) $\boldsymbol{q}^{(1,1)}$ (2nd largest ξ^{μ})

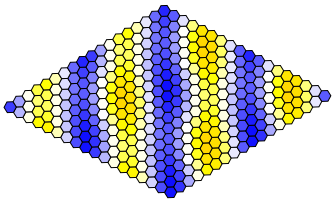

(g) $\boldsymbol{q}^{(2,0)}$ (3rd largest ξ^{μ})

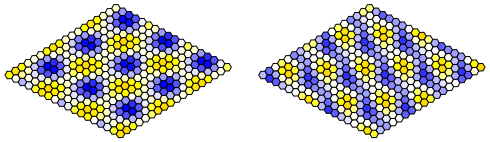

(h) $\boldsymbol{q}^{(3,0)}$ and $\boldsymbol{q}^{(2,2)}$ (5th and 6th largest ξ^{μ}, respectively)

Fig. 9: Spectrum analysis of Region 1 for Southern Germany in 2011. In (c), the red bars correspond to the spectra with the first to the fourth largest eigenvalues ξ^{μ} and the brown bars to others. In (d)–(h), a blue hexagonal area denotes a positive component, a yellow one indicates a negative one, and the magnitude of the component increases as the color becomes darker.

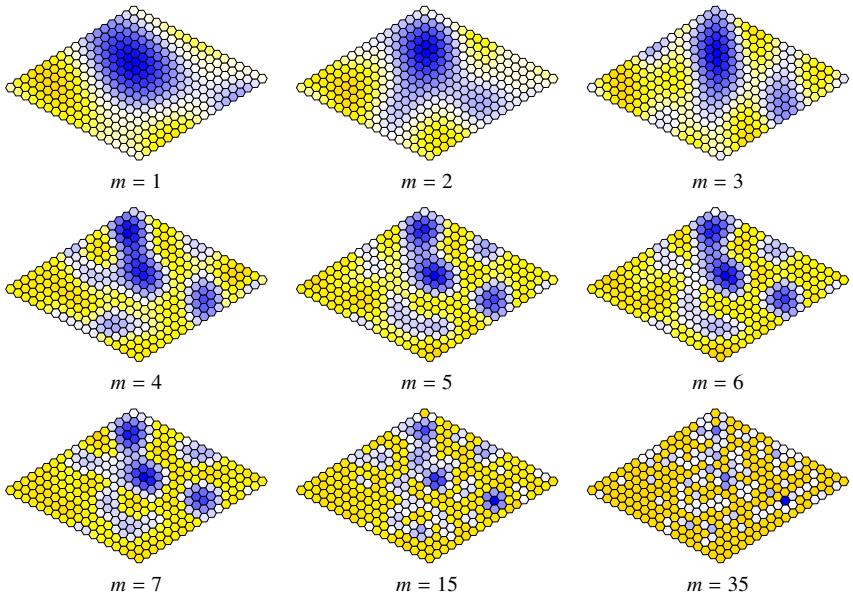

Fig. 10: Vectors $\boldsymbol{q}_m^*$ for principal components for Region 1. A blue hexagonal area denotes a positive component, a yellow one indicates a negative one, and the magnitude of the component increases as the color becomes darker.

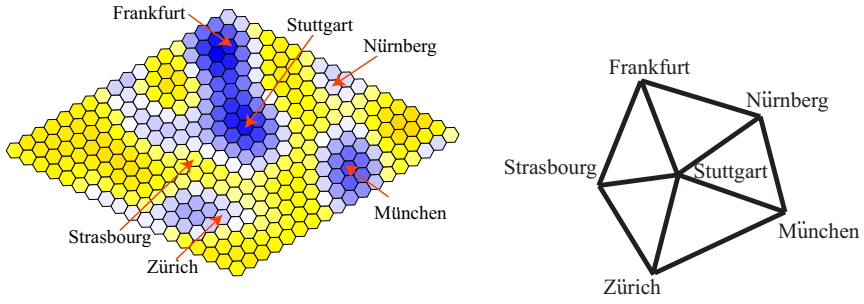

(a) Principal vector $\boldsymbol{q}_4^*$ (b) Christaller's distribution

Fig. 11: Comparison of principal vector $\boldsymbol{q}_4^*$ of Region 1 with Christaller's distribution of cities (Christaller, 1966, p.224–225). At the left, a blue hexagonal area denotes a positive component, a yellow one indicates a negative one, and the magnitude of the component increases as the color becomes darker.

3.3 Time evolution in Southern Germany (Region 1) during 1987 to 2011

We observe the time evolution of the spectra for the incremental population in Southern Germany (Region 1) during the periods 1987–2000 and 2000–2011, which contain an epoch-making event of the German reunification in 1990. In the period 1987–2000, an increase of the population is spread over the northern part of the region (Fig. 12(b)). As shown in Fig. 12(c), there is a strong spectrum for the megalopolis pattern $\boldsymbol{q}^{(1,0)}$, whereas other spectra are similar to those for 2011 in Fig. 9(c).

Such similarity can be also seen in the principal vector $\boldsymbol{q}_4^*$ for the present case in Fig. 12(d) and that in 2011 in Fig. 11(a). The four rhombic cities, München, Frankfurt, Stuttgart, and Nürnberg, display an increase of population proportional to the population in 2011. On the other hand, other agglomerated places, such as Saarbrücken, Strasbourg, and Zürich, display a smaller increase of population. The increase of population in the four large cities can be characterized by the megalopolis pattern $\boldsymbol{q}^{(1,0)}$ in Fig. 12(e), which expresses an agglomeration around the northeastern part of the region encompassing the four large cities.

A phase shift of population increase pattern can be observed in the period 2000–2011; the core–satellite pattern $\boldsymbol{q}^{(2,1)}$ becomes the strongest spectrum (Fig. 13(e)), following the predominance of the megalopolis pattern $\boldsymbol{q}^{(1,0)}$ during 1987–2000. This core–satellite pattern indicates current and future trends of agglomeration to core places, such as München, Frankfurt, Stuttgart, Nürnberg, and so on. The center of this pattern is located on München and an agglomeration to München can be also seen from $\boldsymbol{q}_4^*$ in Fig. 13(d). In this manner, the core of agglomeration shifted from Frankfurt and Stuttgart during 1987–2000 to München during 2000–2011.

Thus, we have successfully arrived at a view of time evolution of agglomerating places. Whereas central place theory is static, the present spectrum analysis procedure presents a quasi-dynamic view based on time evolution of population.

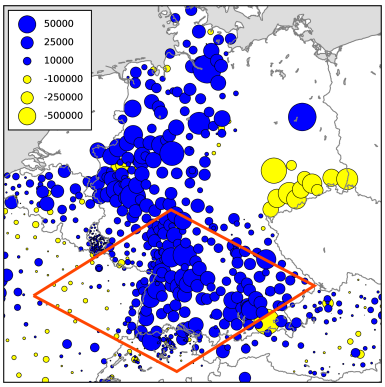

(a) Map of incremental population and Region 1 (red rhombus)

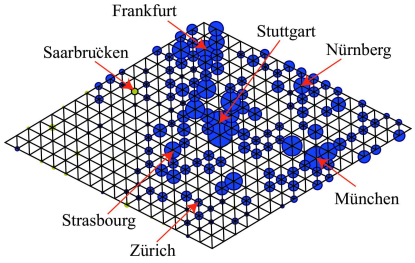

(b) Discretized incremental population

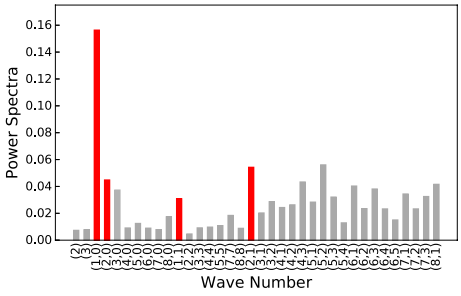

(c) Spectrum

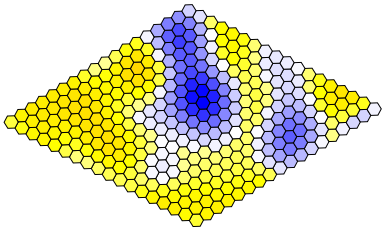

(d) Principal component $\boldsymbol{q}_4^*$

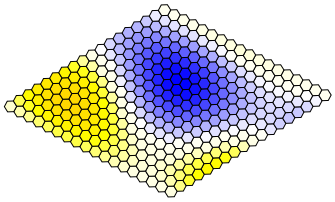

(e) Megalopolis pattern for $\boldsymbol{q}^{(1,0)}$

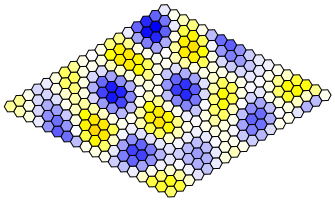

(f) Core–satellite pattern for $\boldsymbol{q}^{(2,1)}$

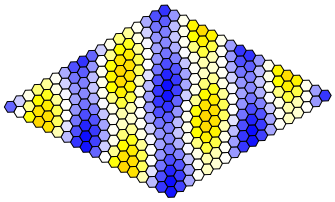

(g) Spatial pattern for $\boldsymbol{q}^{(2,0)}$

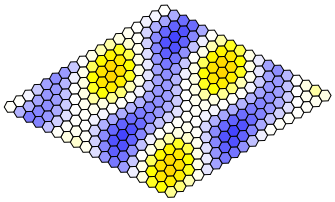

(h) Spatial pattern for $\boldsymbol{q}^{(1,1)}$

Fig. 12: Time evolution of spectra for Region 1 (1987–2000). In (c), the red bars correspond to the spectra with the first to the fourth largest eigenvalues ξ^{μ} and the brown bars to others. In (d)–(h), a blue hexagonal area denotes a positive component, a yellow one indicates a negative one, and the magnitude of the component increases as the color becomes darker.

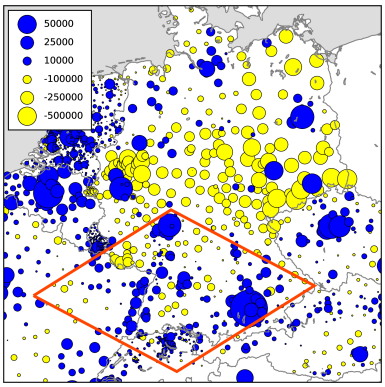

(a) Map of incremental population and Region 1 (red rhombus)

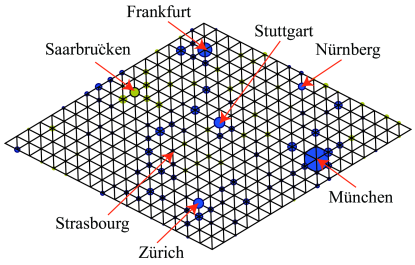

(b) Discretized incremental population

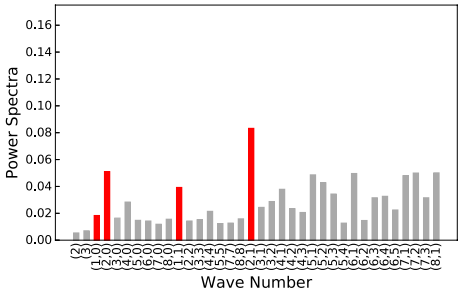

(c) Spectrum

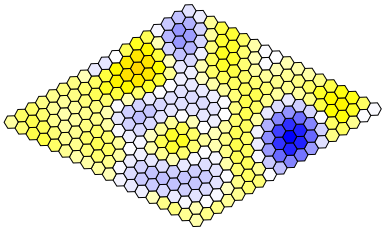

(d) Principal component $\boldsymbol{q}_4^*$

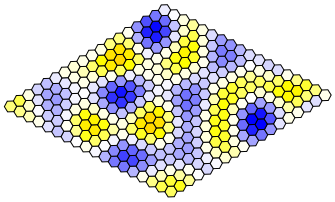

(e) Core–satellite pattern for $\boldsymbol{q}^{(2,1)}$

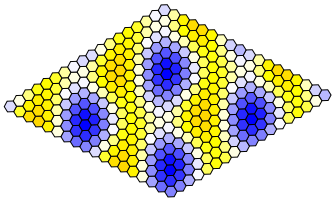

(f) Rhombic pattern for $\boldsymbol{q}^{(2,0)}$

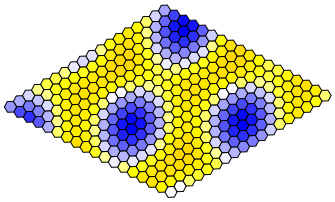

(g) Spatial pattern for $\boldsymbol{q}^{(1,1)}$

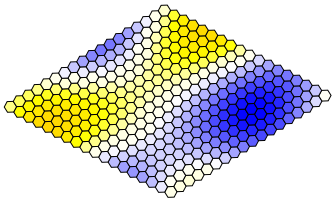

(h) Spatial pattern for $\boldsymbol{q}^{(1,0)}$

Fig. 13: Time evolution of spectra for Region 1 (2000–2011). In (c), the red bars correspond to the spectra with the first to the fourth largest eigenvalues ξ^{μ} and the brown bars to others. In (d)–(h), a blue hexagonal area denotes a positive component, a yellow one indicates a negative one, and the magnitude of the component increases as the color becomes darker.

3.4 Middle Germany (Region 2) in 2011

Figure 14(c) depicts the spectrum for Region 2 of Middle Germany in Fig. 14(b). There is the largest peak for the spectrum for the megalopolis pattern $\boldsymbol{q}^{(1,0)}$ (Fig. 14(e)), accompanied by other peaks for the rhombic pattern $\boldsymbol{q}^{(2,0)}$ (Fig. 14(f)) and the skewed rhombic-like pattern $\boldsymbol{q}^{(1,1)}$ (Fig. 14(g)).

Such predominance of the three strongest spectra for $(k, \ell) = (1, 0)$, $(2, 0)$, and $(1, 1)$ is also observed for the prototype rhombic pattern with a large city, a middle-size city, and two small cities in Fig. 6(b). For Region 2, a large city corresponds to the megalopolis pattern $\boldsymbol{q}^{(1,0)}$ around Köln (Fig. 14(e)) and a middle-size one to Frankfurt. The rhombic pattern $\boldsymbol{q}^{(2,0)}$ with the second largest spectrum has four agglomerated places (Fig. 14(f)): two of them are in good agreement with the locations of Köln and Frankfurt but the other two are not necessarily in good agreement with the real city distribution.

In search of a better correspondence with real city distribution, we resort to the principal vector $\boldsymbol{q}_4^*$ in Fig. 14(d), which displays four blue zones of agglomeration forming a distorted rhombic shape comprising four cities: Köln, Saarbrücken, Frankfurt, and Hanover. (See Fig. 15 for $\boldsymbol{q}_m^*$ for various values of m.)

By combining this rhombic pattern with the core–satellite-like pattern for Region 1 expressed also by the principal vector (Fig. 11(a)), we can construct the spatial network of cities in Germany shown in Fig. 16, thereby demonstrating the usefulness of the principal vector. The pattern is skewed towards southwest due to the geographical borders of the Alps in the south and Rhine River, Schwarzwald, and Vosges in the west.

3.5 Time evolution in Middle Germany (Region 2) during 1987 to 2011

In the period of 1987–2000, there is a spread increase of population (Fig. 17(b)). The spectrum in Fig. 17(c) has a sharp peak for the megalopolis pattern $\boldsymbol{q}^{(1,0)}$ (Fig. 17(e)), expressing a large agglomeration around Köln, similarly to the spectrum analysis for 2011 (Fig. 14).

A phase shift was observed in the period 2000–2011; there is a large decrease of population (Fig. 18(b)), unlike an overall increase in 1987–2000. The spectrum in Fig. 18(c) displays peaks with similar magnitudes for several principal components $(k, \ell) = (1, 0)$, $(1, 1)$, $(2, 0)$, and $(2, 1)$. Among these, we refer to $\boldsymbol{q}^{2,1}$ with the strongest spectrum (Fig. 18(e)), which expresses a reversed core–satellite pattern centered around Köln with a large decrease. This captures the pattern of the principal vector $\boldsymbol{q}_4^*$ in Fig. 18(d) fairly well. Thus the agglomeration around Köln shifts from an increase during 1986–2000 to a decrease during 2000–2011.

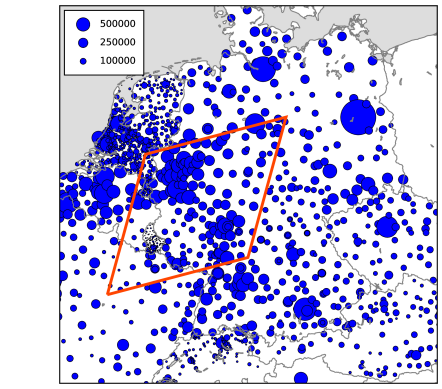

(a) Population map and Region 2 (red rhombus)

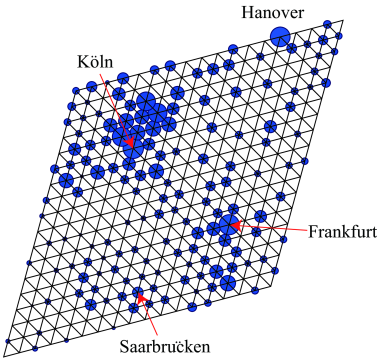

(b) Discretized population

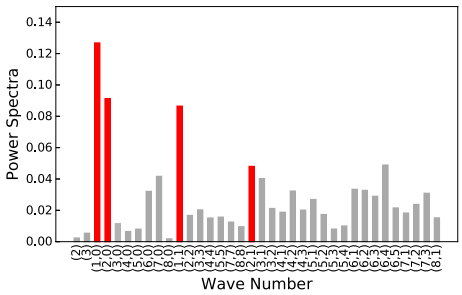

(c) Spectrum

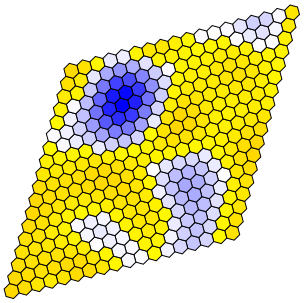

(d) Principal component $\boldsymbol{q}_4^*$

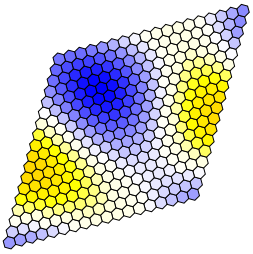

(e) Megalopolis pattern for $\boldsymbol{q}^{(1,0)}$

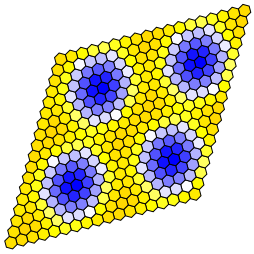

(f) Rhombic pattern for $\boldsymbol{q}^{(2,0)}$

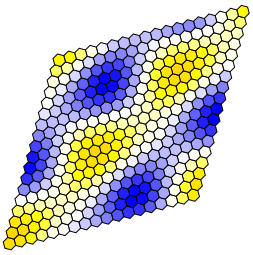

(g) Skewed rhombic pattern for $\boldsymbol{q}^{(1,1)}$

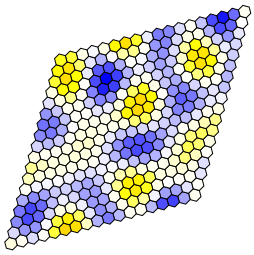

(h) Spatial pattern for $\boldsymbol{q}^{(2,1)}$

Fig. 14: Spectrum analysis of Region 2 for Middle Germany in 2011. In (b), a blue circle denotes the size of population. In (c), the red bars correspond to the spectra with the first to the fourth largest eigenvalues ξ^μ and the brown bars to others. In (d)–(h), a blue hexagonal area denotes a positive component, a yellow one indicates a negative one, and the magnitude of the component increases as the color becomes darker.

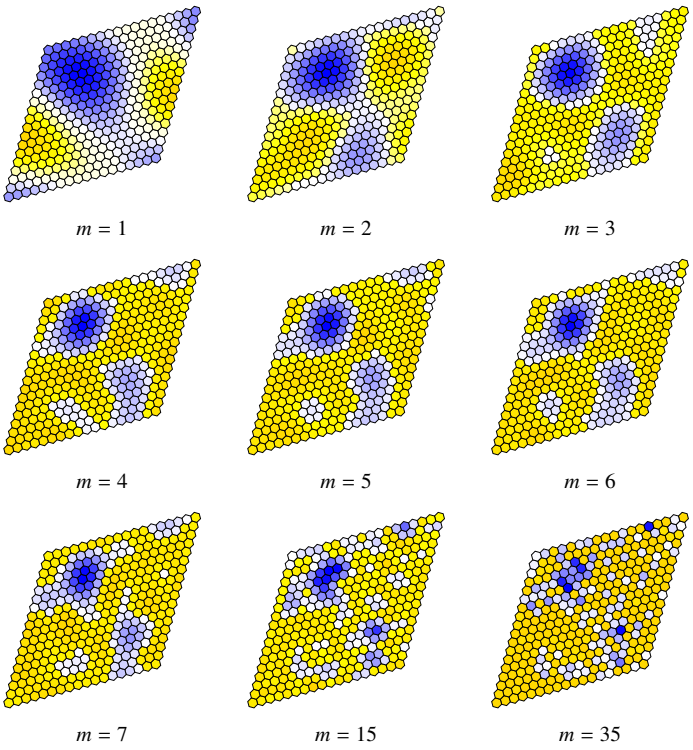

Fig. 15: Vectors $\boldsymbol{q}_m^*$ for principal components for Region 2. A blue hexagonal area denotes a positive component, yellow one indicates a negative one, and the magnitude of the component increases as the color becomes darker.

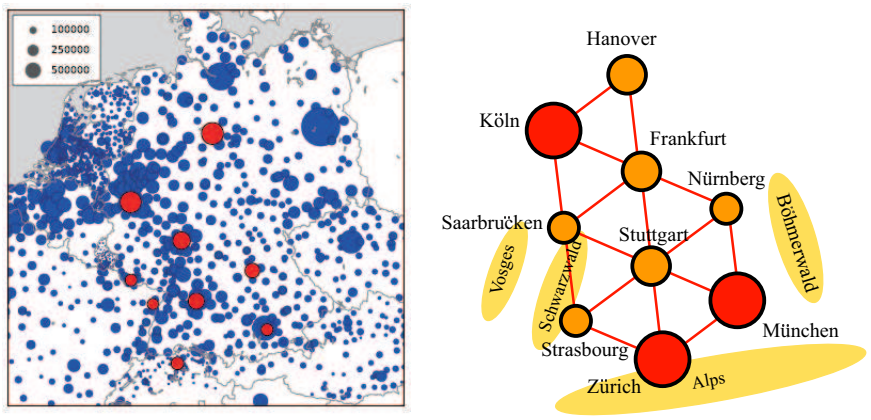

Fig. 16: Spatial network of cities in Germany. At the left, circles indicate the size of population and red circles expresses the location of major cities that appear in the network at the right, a blue circle denotes a positive component, and the area of a circle expresses the magnitude of the component.

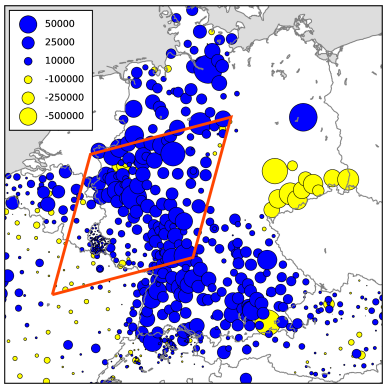

(a) Map of incremental population and Region 2 (red rhombus)

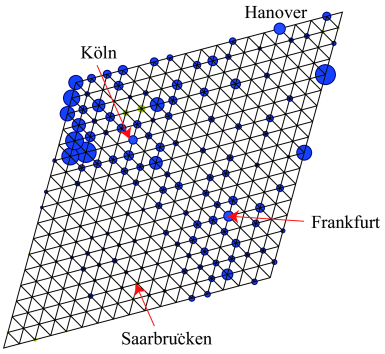

(b) Discretized incremental population

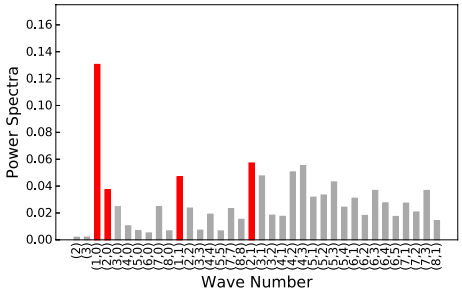

(c) Spectrum

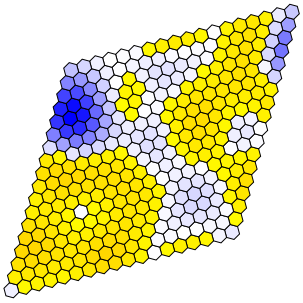

(d) Principal component $\boldsymbol{q}_4^*$

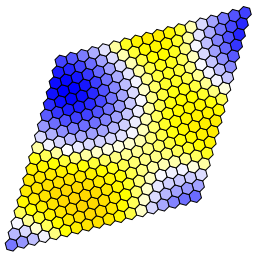

(e) Megalopolis pattern for $\boldsymbol{q}^{(1,0)}$

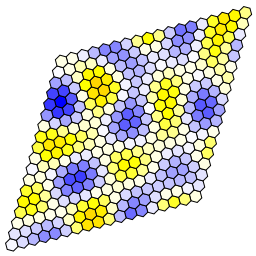

(f) Core–satellite pattern for $\boldsymbol{q}^{(2,1)}$

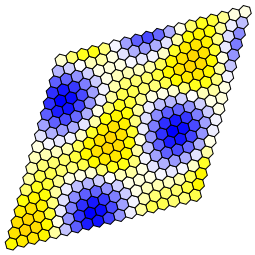

(g) Spatial pattern for $\boldsymbol{q}^{(1,1)}$

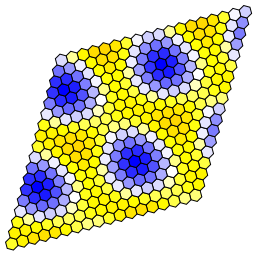

(h) Spatial pattern for $\boldsymbol{q}^{(2,0)}$

Fig. 17: Time evolution of spectra for Region 2 (1987–2000). In (c), the red bars correspond to the spectra with the first to the fourth largest eigenvalues ξ^{μ} and the brown bars to others. In (d)–(h), a blue hexagonal area denotes a positive component and a yellow one indicates a negative one, and the magnitude of the component increases as the color becomes darker.

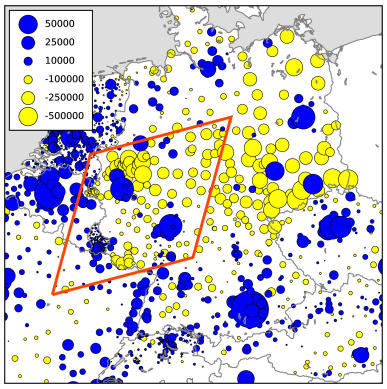

(a) Map of incremental population and Region 2 (red rhombus)

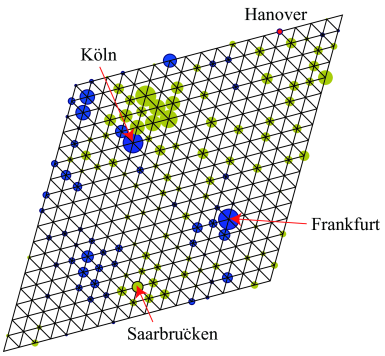

(b) Discretized incremental population

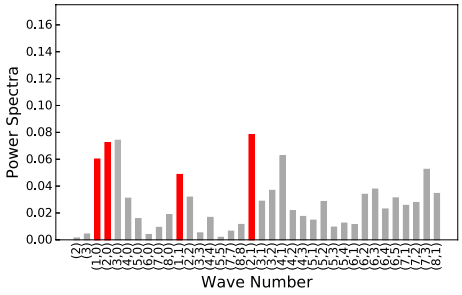

(c) Spectrum

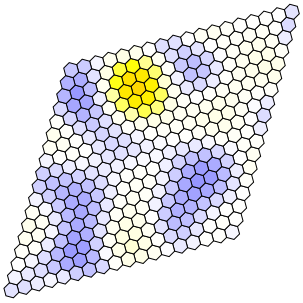

(d) Principal component $\boldsymbol{q}_4^*$

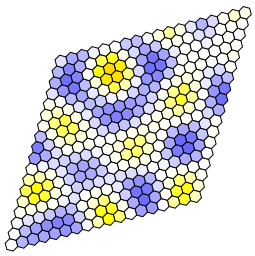

(e) Core–satellite pattern for $\boldsymbol{q}^{(2,1)}$

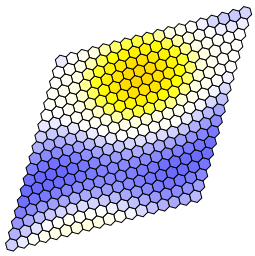

(f) Megalopolis pattern for $\boldsymbol{q}^{(1,0)}$

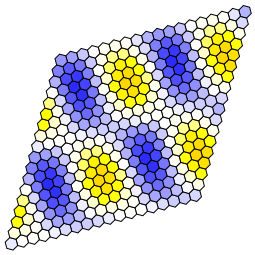

(g) Spatial pattern for $\boldsymbol{q}^{(2,0)}$

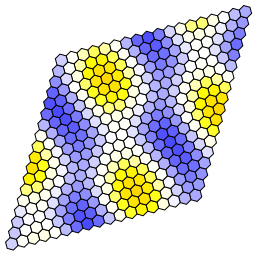

(h) Spatial pattern for $\boldsymbol{q}^{(1,1)}$

Fig. 18: Time evolution of spectra for Region 2 (2000–2011). In (c), the red bars correspond to the spectra with the first to the fourth largest eigenvalues ξ^{μ} and the brown bars to others. In (d)–(h), a blue hexagonal area denotes a positive component and a yellow one indicates a negative one, and the magnitude of the component increases as the color becomes darker.

4 Conclusions

We utilized a group-theoretic double Fourier spectrum analysis procedure (Ikeda et al., 2018) as a systematic means to capture characteristic agglomeration patterns in population data. We have newly introduced the *principal vector* as a means to grasp agglomeration patterns. We set forth benchmark spectra for important spatial patterns that are to be sought for in the spectrum in population data. Such benchmark spectra and associated spatial patterns were actually found in the population data in Germany in 2011 and spatial agglomerations were successfully grasped by the principal vector. An incremental population during the pre- and post-reunification periods (from 1987 to 2011) was investigated using this vector to successfully detect a shift of predominant population increase/decrease patterns.

Despite its importance, the value of m for the principal vector was chosen empirically based on the analysis of the benchmark spectra in Section 2.3. In the experience of this paper, the use of $m = 4$ terms is sufficient to capture characteristic agglomeration patterns in the real population data in Germany. Thus the number of terms required is very small in comparison with the total number of 18×18 (= 324) terms of the Fourier analysis. It would be a future topic to develop a concrete methodology to determine the threshold value of m to capture characteristic agglomeration patterns.

References

Banaszak, M., Dziecielski, M., Nijkamp, P., Ratajczak, W., 2015. Self-organisation in spatial systems: From fractal chaos to regular patterns and vice versa. PLOS ONE 10 (9): e0136248.

Barbero and Zofío, 2016. The multiregional core-periphery model: The role of the spatial topology. Networks and Spatial Economics 16, 469–496.

Bosker, M., Brakman, S., Garretsen, H., Schramm, M., 2008. A century of shocks: The evolution of the German city size distribution 1925–1999. Regional Science and Urban Economics 38 (4), 330–347.

——. 2010. Adding geography to the new economic geography: bridging the gap between theory and empirics. Journal of Economic Geography 10 (6), 793–823.

Christaller, W., 1933. Die zentralen Orte in Süddeutschland. Gustav Fischer. English translation: 1966. Central Places in Southern Germany. Prentice Hall.

Clarke, M., Wilson, A. G., 1983. The dynamics of urban spatial structure: Progress and problems. Journal of Regional Science 23 (1), 1–18.

Dray, S., Legendre, P., Peres-Neto, P. R., 2006. Spatial modelling: a comprehensive framework for principal coordinate analysis of neighbour matrices (PCNM), Ecological Modelling 196, 483–493.

Ducruet, C., Beauguitte, L., 2014. Spatial science and network science: Review and outcomes of a complex relationship. Networks and Spatial Economics 14, 297–316.

Eaton, B. C., Lipsey, R. G., 1975. The principle of minimum differentiation reconsidered: Some new developments in the theory of spatial competition. The Review of Economic Studies 42 (1), 27–49.

Findeisena, S., Südekum, J., 2008. Industry churning and the evolution of cities: Evidence for Germany. Journal of Urban Economics 64 (2), 326–339.

Fujita, M., Krugman, P., Mori, T., 1999. On the evolution of hierarchical urban systems. European Economic Review 43 (2), 209–251.

Golubitsky, M., Stewart, I., Schaeffer, D. G., 1988. Singularities and Groups in Bifurcation Theory, Vol. 2, Springer-Verlag.

Ikeda, K., Murota, K., 2014. Bifurcation Theory for Hexagonal Agglomeration in Economic Geography, Springer-Verlag.

Ikeda, K., Murota, K., Akamatsu, T., Kono, T., Takayama, Y., 2014. Self-organization of hexagonal agglomeration patterns in new economic geography models. Journal of Economic Behavior & Organization 99, 32–52.

Ikeda, K., Murota, K., Takayama, Y., 2017. Stable economic agglomeration patterns in two dimensions: Beyond the scope of central place theory. Journal of Regional Science 57 (1), 132–172.

Ikeda, K., Takayama, Y., Onda, M., Murakami, D., 2018. Group-theoretic spectrum analysis of population distribution in Southern Germany and Eastern USA. International Journal of Bifurcation and Chaos 28 (14),18300458.

Lösch, A., 1940 *Die räumliche Ordnung der Wirtschaft*, Gustav Fischer.

Mulligan, G. F., Partridge, M. D., Carruthers, J. I., 2012. Central place theory and its reemergence in regional science. The Annals of Regional Science 48 (2), 405–431.

Munz, M., Weidlich. W., 1990. Settlement formation, Part II: Numerical simulation. The Annals of Regional Science 24, 177–196.

Murakami, D., Griffith, D. A., 2015. Random effects specifications in eigenvector spatial filtering: a simulation study, J. Geographical Systems 17, 311–331.

Redding, S. J., Sturm, D. M., 2008. The costs of remoteness: Evidence from German division and reunification. The American Economic Review 98 (5), 1766–1797.

Sanglier, M., Allen, P., 1989. Evolutionary models of urban systems: An application to the Belgian provinces. Environment and Planning A 21, 477–498.

Stelder, D., 2005. Where do cities form? A geographical agglomeration model for Europe. Journal of Regional Science 45, 657–679.

Tabuchi, T., Thisse, J. F., 2011. A new economic geography model of central places. Journal of Urban Economics 69, 240–252.

Tiefelsdorf, M., Griffith, D. A., 2007. Semiparametric filtering of spatial autocorrelation: the eigenvector approach, Environment Planning A 39, 1193–1221.